Representation of Clouds and Precipitation Processes in the Community Atmosphere Model Version 3 (CAM3)

BYRON A. BOVILLE, PHILIP J. RASCH, JAMES J. HACK, AND JAMES R. MCCAA

National Center for Atmospheric Research, Boulder, Colorado*

(Manuscript received 23 January 2005, in final form 14 September 2005)

ABSTRACT

The parameterizations of clouds and precipitation processes have been revised considerably in the Community Atmosphere Model version 3 (CAM3) compared to its predecessors, CAM2 and the Community Climate Model version 3 (CCM3). The parameterizations in CAM3 are more realistic in their representation of processes affecting cloud liquid and ice particles and represent the linkages between processes more completely. This paper describes the changes to the representation of clouds in CAM3, including the partitioning of cloud water between liquid and ice phases, the determination of particle sizes and sedimentation rates, the phase and evaporation rate of precipitation, and the calculation of the cloud fraction.

Parameterization changes between CCM3 and CAM2 introduced a significant cold bias at the tropical tropopause, resulting in a dry bias for stratospheric water vapor. Tests of the sensitivity of the tropical temperature profile and the tropical tropopause temperature to individual process changes suggested that the radiative balance at the tropopause was altered by improvements in both clouds and relative humidity below. Radiative equilibrium calculations suggested that the cold bias could be removed by improving the representation of subvisible cirrus clouds. These results motivated the complete separation of the representation of liquid and ice cloud particles and an examination of the processes that determine their sources and sinks. As a result of these changes, the tropopause cold bias has been almost eliminated in CAM3.

The total cloud condensate variable, used in CAM2, has been separated into cloud liquid and cloud ice variables in CAM3. Both sedimentation and large-scale transport of the condensate variables are now included. Snowfall is computed explicitly and the latent heat of fusion has been included for all freezing and melting processes. Both deep and shallow convection parameterizations now detrain cloud condensate directly into the stratiform clouds instead of evaporating the detrained condensate into the environment. The convective parameterizations are not easily modified to include the latent heat of fusion. Therefore, the determination of the phase of convective precipitation, and of detrained condensate, is added as a separate step. Evaporation is included for sedimenting cloud particles and for all sources of precipitation.

1. Introduction

Clouds are extremely complex phenomena whose representation in general circulation models (GCMs) is necessarily simplified. Early GCMs (e.g., Holloway and Manabe 1971) treated volumes of air as clear or cloudy, depending on whether the average relative humidity exceeded 100%. The properties of clouds (extent, thickness, seasonality) were prescribed independently of the atmospheric state. As climate modeling has matured, the complexity of cloud representations in GCMs has increased. Cloud processes are being treated with increasing realism, with much greater attention to the physical basis and the internal consistency of their representation. This paper addresses the treatment of clouds in the Community Atmosphere Model version 3 (CAM3: Collins et al. 2006b), which is another step toward the goal of a completely consistent, physically based, comprehensive representation for cloud processes.

CAM3 is the atmospheric component of the Community Climate System Model version 3 (CCSM3: Collins et al. 2006a), which is used for coupled ocean–atmosphere studies, including climate change studies. A major emphasis in developing CAM3 was to improve the treatment of clouds, especially ice clouds, compared

* The National Center for Atmospheric Research is sponsored by the National Science Foundation.

Corresponding author address: Dr. Byron Boville, NCAR, P.O. Box 3000, Boulder, CO 80307.
E-mail: boville@ucar.edu

to CAM2 (Collins et al. 2002; Boville and Bretherton 2003) and to provide new mechanisms for interactions between cloud properties and the other components of the model. CAM2 included the prognostic cloud water formulation of Rasch and Kristjánsson (1998, hereafter RK98), which represented total cloud condensate (liquid + ice) with a single variable and ignored both advection and gravitational settling of cloud particles. To treat clouds more accurately, several major changes were made in CAM3: the total cloud condensate variable was separated into cloud liquid and ice variables; the cloud liquid and ice are transported by the circulation; gravitational settling of cloud ice and liquid particles is now represented; ice and liquid particle sizes are temperature dependent and are treated consistently for sedimentation and radiative properties; the phase of cloud condensate and precipitation is determined explicitly for all processes and the latent heat of fusion is included, to ensure energy conservation; and the deep and shallow convection schemes are now linked to the stratiform clouds through detrainment of cloud liquid and ice. The main purpose of this manuscript is to document the changes to the cloud process in CAM3 and the reasons they were introduced. Extensive discussions of the hydrologic cycle can be found in Hack et al. (2006), for the mean, and in Rasch et al. (2006) for the variability.

A significant new bias in CAM2 compared to its predecessor, the Community Climate Model version 3 (Kiehl et al. 1998), was an ~3 K cooling of the tropical tropopause. CCM3 obtained a reasonably accurate tropical tropopause temperature and also simulated stratospheric water vapor reasonably when methane transport and oxidation was included (Boville et al. 2001). The cooling of the tropopause in CAM2 resulted in an unrealistic drying of the stratosphere. The radiative impact of a dryer stratosphere is relatively modest and most GCMs do not even bother to include the methane source, which accounts for ~50% of stratospheric water vapor. However, chemical modeling is a major application of CAM3 and this error becomes very important when stratospheric chemical processes are included, as in Sassi et al. (2005). Each of the major parameterization changes between CCM3 and CAM2 contributed to the tropopause cooling, but each is believed to represent an improvement in the representation of the physical system. The tropopause cooling exposed remaining deficiencies in the treatment of clouds in CAM2 and motivated a thorough investigation of the treatment of cloud ice and of the coupling between the moist processes in developing CAM3. Improvements in the treatment of cloud ice in CAM3, particularly very thin cirrus near the tropical tropopause, removed most of the tropopause cold bias.

The models used in this study are briefly described in section 2. The tropical tropopause bias in CAM2 and the effect of subvisible cirrus are discussed in section 3. A series of improvements to the treatment of cloud water, precipitation phase, and cloud fraction are described in section 4, and their effect on the CAM3 simulation is described in section 5. Conclusions appear in section 6.

2. Model description

CAM3 is closely related to its immediate predecessors, CAM2 and CCM3. Several of the physical parameterizations are essentially unchanged from CCM3. Boundary-layer-rooted deep convection is parameterized following Zhang and McFarlane (1995, hereafter ZM95). Shallow and upper-level convection uses Hack (1994, hereafter H94). Holtslag and Boville (1993) is used for the boundary layer, and orographically generated gravity waves closely follow McFarlane (1987).

The principal changes in physical parameterizations between CCM3 and CAM2 were 1) evaporation of precipitation from ZM95 convection following Sundqvist (1988), which moistens the tropical middle troposphere; 2) an updated longwave radiation treatment of water vapor by Collins et al. (2002), which increases cooling in the upper troposphere; and 3) the RK98 treatment of stratiform cloud as modified by Zhang et al. (2003), which includes predicting the total (liquid + ice) cloud condensate. Other changes to the parameterizations had a modest impact on the simulation and are described in Collins (2001), Williamson (2002), and Boville and Bretherton (2003).

Changes to the moist processes between CAM2 and CAM3 are described in section 4. In addition, Collins et al. (2006c) updated radiation parameters using new line-by-line databases, with minor impact on the simulation. Other parameterizations are identical in CAM2 and CAM3.

Three dynamical cores are supported in CAM3: the spectral core used in CCM3; the semi-Lagrangian core of Williamson and Olson (1994); and the finite volume core of Lin (2004). The spectral core is presently used for coupled ocean–atmosphere studies but the finite volume core has significant advantages for tracer transport (including cloud condensate) and is used here. The finite volume core uses a regular latitude–longitude grid and most work is done at a resolution of $2^\circ \times 2.5^\circ$, although some sensitivity tests below used $4^\circ \times 5^\circ$. The standard vertical resolution for tropospheric studies uses 26 layers with a maximum spacing of 0.16 scale heights (~1.1 km) in the troposphere.

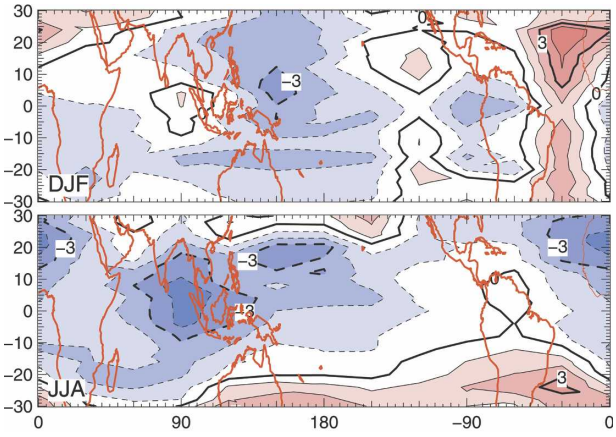

FIG. 1. Cold point tropopause temperature bias for CAM2 compared to GPS/MET observations for (top) DJF and (bottom) JJA. The contour interval is 1 K.

3. Tropical tropopause cold bias

The cold point tropopause (CPT), defined as the coldest point in the temperature profile, is commonly used in tropical tropopause studies (e.g., Seidel et al. 2001). The seasonal cycle of the CPT temperatures is believed to determine the concentration of water vapor in the air entering the stratosphere, although the precise mechanisms are still subject to debate (Sherwood 2000; Dessler 1998; Holton and Gettelman 2001). Water vapor is critically important in stratospheric chemistry because it is the main source of HO_x. Less stratospheric water vapor tends to result in more stratospheric ozone.

Figure 1 shows the difference between CPT temperatures simulated by CAM2 and those observed using the Global Positioning System Meteorology (GPS/MET: Randel et al. 2003) during April 1995–February 1997 and May 2001–June 2002. The CAM2 bias is almost entirely negative and is larger in June–August (JJA) than in December–February (DJF). The largest cold biases tend to occur in the regions of the coldest CPT, the west Pacific in DJF and Indonesia/Indian Ocean in JJA. Cooling of the CPT was one of the major biases introduced between CCM3 and CAM2. It should be noted that the CPT temperature bias with respect to climatology is probably somewhat larger than shown in Fig. 1. The GPS/MET observations are for a particularly cold year at the CPT (Randel et al. 2003): they are used here because they provide full coverage of the Tropics, unlike the radiosonde observations used in the climatology of Seidel et al. (2001).

The CAM2 simulation in Fig. 1 used the finite volume dynamical core of Lin (2004) at 2° × 2.5° horizontal resolution. The CPT is slightly colder for the other two dynamical cores supported in CAM2 but otherwise the biases are similar for all three cores at all horizontal resolutions tested.

The CPT in CAM2 forms at the 85-mb level for almost all tropical grid points in all seasons. According to Seidel et al. (2001), the observed CPT pressure varies geographically and seasonally, but averages ~90 mb in DJF and ~100 mb in JJA. Although CAM2 has relatively high vertical resolution in the vicinity of the tropopause, the observed annual range is less than the vertical grid spacing (~15 mb). Properly representing the horizontal and annual variation of the CPT temperature and pressure would require a vertical resolution of <5 mb, or ~400 m.

a. Response to parameterization changes

The contribution to the CPT bias by the major parameterization changes from CCM3 to CAM2 is shown in Table 1. These results were obtained from 5-yr simulations using the finite volume dynamical core at 4° × 5° resolution. The parameterization results were obtained by replacing CAM2 parameterizations with the previous versions from CCM3 for longwave radiation, evaporation of ZM95 convective precipitation (not present in CCM3), and stratiform cloud. The CCM3 results were obtained by using the entire CCM3 parameterization suite with the finite volume core.

The largest impact came from evaporation of ZM95 convective precipitation with smaller impacts from the longwave radiation and stratiform cloud. Note the combination of the three changes is 50% larger than the net difference between CCM3 and CAM2. The cold bias in CAM2 would have been even larger except for the additional parameterization changes mentioned above.

Figure 2 shows profiles of the January equatorial temperature differences between CAM2, CCM3, and the intermediate model versions. The maximum temperature difference occurs near the CPT (shown by large filled symbols) in each case, although comparable differences are found below 500 mb for the evaporation of convective precipitation. The three parameterization

TABLE 1. Tropopause (cold point) temperatures (K) and difference compared to CAM2.

	T	ΔT
CAM2	187.2	
GPS/MET	189.1	1.9
CCM3	190.1	2.9
Stratiform cloud	187.8	0.6
Convective evaporation	188.5	1.3
Longwave radiation	188.2	1.0
All 3	191.8	4.6

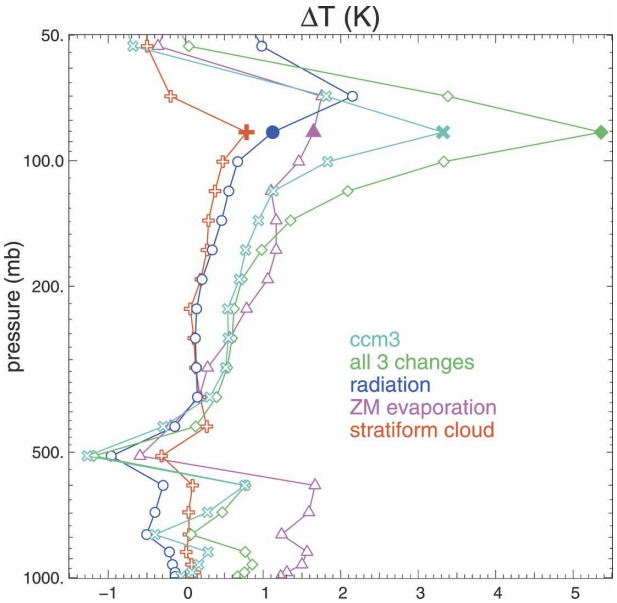

FIG. 2. Equatorially (8°S–8°N) averaged temperature differences compared to CAM2 for CCM3 (diamonds) and CAM2 using the CCM3 parameterization of radiation (circles), evaporation of ZM95 precipitation (diamonds), and stratiform cloud (crosses).

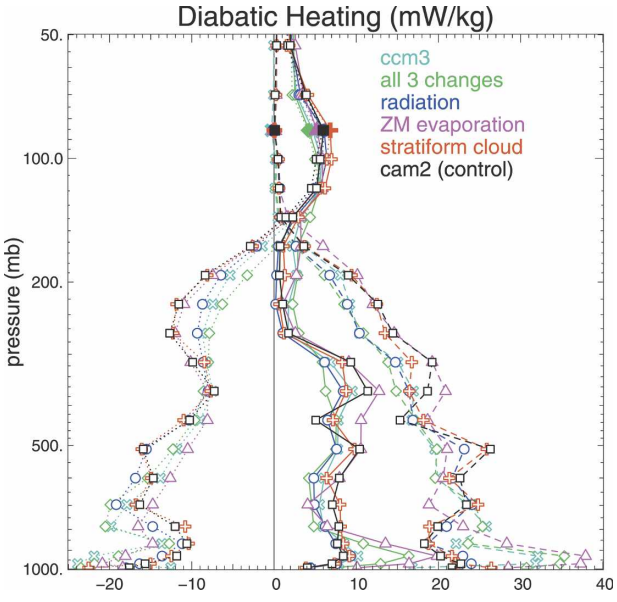

FIG. 3. As in Fig. 2 except that the net diabatic heating (mW kg^{-1}) profiles are shown and the CAM2 control is included (boxes). Also shown are the radiative heating rates (dotted lines) and the turbulent heating rates (dashed lines).

changes tend to offset each other except near the tropopause where they each have the same sign.

In the lower and middle troposphere, there are substantial changes in the tropical diabatic heating when the parameterizations are changed (Fig. 3). All parameterized heating except radiation is included in the turbulent heating term. Note that 1 mW kg^{-1} heating corresponds to a temperature tendency of 0.08 K day^{-1}. The stratus cloud produces the smallest changes in the heating rates and in the temperature profile, while the evaporation of convective precipitation produces the largest changes. The longwave radiation affects only the radiative heating term directly, while the ZM95 evaporation affects only the turbulent heating directly. The stratus clouds affect turbulent heating through latent heat release and radiative heating through cloud properties. In each case, there is a significant, and generally opposing, response in both terms so that the net diabatic heating change is reduced. Changes in the net diabatic heating are balanced primarily be changes in the mean upwelling rate in the Hadley circulation.

As pointed out by Collins et al. (2002), the new longwave radiation increases the radiative cooling between 400 and 200 mb, where the gradient of water vapor is substantial and concentrations are relatively low. A clear separation can be seen between the three cases with the CAM2 radiation and the three cases with the CCM3 radiation. The radiative cooling increase is largely balanced by changes in turbulent (primarily deep convective) heating so that the net diabatic heating change is relatively small.

The changes in the tropical diabatic heating profile are small above 150 mb (~1 mW kg^{-1}), even though the temperature changes are largest there. The only significant heating above 150 mb comes from radiation, which is composed of comparable contributions from the solar and longwave terms between 150 and 70 mb (not shown, note that the longwave term heats that region due to the cold temperatures there). The solar term is almost identical above 150 mb in all cases, since it depends primarily on ozone heating, and the ozone profile is specified.

The near invariance of the longwave heating at the tropopause is more remarkable, since the local emission depends on temperature, and the tropopause temperatures change significantly. The other terms in the longwave heating are absorption of the upwelling and downwelling longwave fluxes. The downwelling flux near the tropopause is independent of the tropospheric parameterization changes, while the upwelling flux is not. Increased midtropospheric humidity, cloud water content, and water vapor absorption all act to reduce the upwelling longwave flux at the tropopause in CAM2 compared to CCM3.

In these simulations, the tropopause temperatures are adjusting to changes in the upwelling longwave flux in order to produce nearly the same net heating rate. This result is not obvious, but might be expected since

it is believed that the upwelling rate at the tropopause is determined by the large-scale dynamics (e.g., Holton et al. 1995). The temperature profile must adjust to produce a radiative heating rate consistent with the adiabatic cooling.

Thin cirrus clouds can strongly affect the radiative balance near the tropopause and the response to radiative perturbations below. These clouds are quite common near the tropopause (e.g., Wang et al. 1996) and tend to be strongly heating. Underestimating either the fractional coverage or ice content of these clouds could easily explain a CPT cold bias.

b. Radiative equilibrium calculations

We now examine the temperature response to heating perturbations of the magnitude that might be expected from tropopause-level cirrus clouds. Given the above argument that all terms except the longwave radiation are nearly invariant at the tropopause, it is instructive to examine the equilibrium response to a radiative heating perturbation using an interactive longwave radiation column model. The inputs to the model are the temperature, humidity, clouds, and trace gases averaged over a day in January from the CAM2 simulation. The longwave cooling Q calculated for the initial profiles is assumed to be balanced by other diabatic terms and adiabatic expansion. Therefore the negative of the initial longwave cooling is taken as a fixed forcing term $-Q_0$ to which a perturbation δ can be applied. The temperature T is advanced,

$$\frac{\partial T}{\partial t} = -Q_0 + \delta + Q(t), \tag{1}$$

until a new equilibrium state is reached. The specific humidity and cloud properties are held fixed. The column model is run for every column in the latitude range $\pm 10^\circ$ and the area average response is computed.

Figure 4 shows the equilibrium T response for cases in which $\delta = 1$ mW kg^{-1} was applied uniformly in the vertical and only between 150–80 mb. Even for a uniform heating, the temperature response is largest at the tropopause (7.5 K) because the radiative relaxation time is longest there due to the cold temperatures. This case is quite unrealistic since heating perturbations in the lower and middle troposphere involve complex feedbacks among parameterizations. The tropopause temperature response is amplified by increased upwelling longwave flux from the warmer temperatures below.

Applying a 1 mW kg^{-1} heating perturbation only over 150–80 mb is more realistic since longwave radiation is the only parameterization that can vary significantly in that domain. The response (~4 K) is comparable to the responses seen in Fig. 2 for the parameterization changes. The response decreases rapidly below the forcing region.

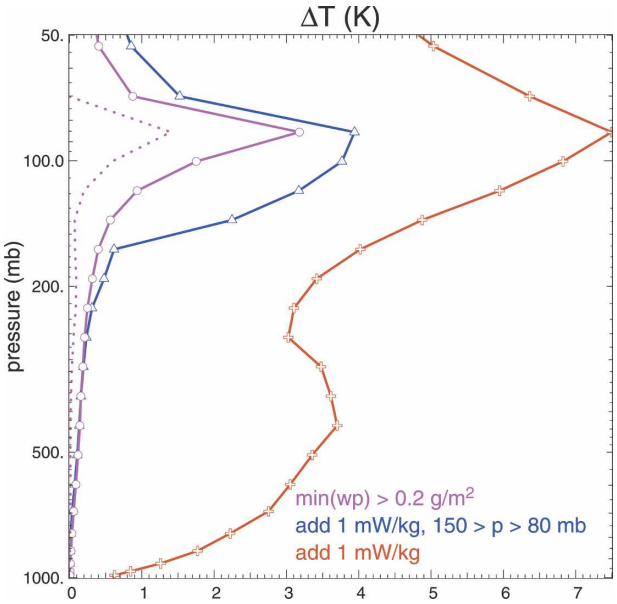

FIG. 4. Radiative equilibrium (200 day) temperature response (K) to adding 1 mW kg^{-1} heating everywhere (crosses), adding 1 mW kg^{-1} for $150 > p > 80$ (triangles), and setting the minimum cloud water path to 0.2 g m^{-2} (circles). The dotted line shows the initial heating perturbation (mW kg^{-1}) for the cloud water path change.

McFarquhar et al. (2000) showed that very thin cirrus clouds observed near the tropopause have longwave heating rates of ~10 mW kg^{-1}. Hartmann et al. (2001) showed that subvisible cirrus clouds (optical depths 0.01–0.05) at the tropopause warm strongly (15–60 mW kg^{-1}) with clear sky below, but may cool slightly (2–13 mW kg^{-1}) with thick anvils below. CAM2 typically has very low cloud water content ($\ll 10^{-4}$ g m^{-3}) near the tropopause due to inconsistencies in the cloud water and fraction formulations, described below.

Figure 4 shows a CPT increase of 3 K due to a small increase in the water content of the thinnest cirrus clouds. All clouds with water path (water content integrated across a layer) between 5×10^{-4} and 0.2 g m^{-2} had their water path reset to 0.2. This corresponds to setting the minimum water content of a cirrus cloud to 1.5×10^{-4} g m^{-3} with an optical depth of 0.015, comparable to the optical depths used by Hartmann et al. (2001). Under clear sky conditions these clouds should heat the tropopause by ~10 mW kg^{-1}. The largest heating change for any column is actually 11 mW kg^{-1}, for a column with 90% cloud cover at 85 mb, but effectively zero cloud water content. The average heating increase

is 1 mW kg^{-1} due to columns without tropopause cirrus and columns with thick cloud below. Both the heating rates and temperature change are comparable to those obtained by Rosenfield et al. (1998) for subvisible cirrus in a two-dimensional model.

The stratiform cloud parameterization in CAM2 predicts the water content inside clouds but conserves the cell average water content across time. A decrease in cloud fraction between time steps results in an increase of the in-cloud water content, which will tend to produce both evaporation and precipitation of cloud water. As in CCM3, CAM2 diagnoses the cloud fraction based on relative humidity and stability. The upper tropical troposphere is quite stable, so the cloud fraction varies from 0 to 1 over a relative humidity range of 1%. Thus, even minor variations in temperature will cause the cloud fraction to switch between 1 and 0, resulting in a dramatic increase of in-cloud water content and conversion of cloud ice particles to precipitate.

The powerful impact of cirrus clouds on the tropopause temperature, together with the cirrus cloud problems in CAM2, were among the main motivating factors leading to a thorough examination of the connections between the moist parameterizations in CAM2 and the role of cloud ice.

4. Changes to the model

Here we describe the treatment of moist processes in CAM3, particularly as they relate to stratiform cloud water content, and the differences with respect to CAM2 and CCM3. Including the latent heat of fusion in the convection schemes would have required major conceptual changes. Therefore, the convection schemes were left unchanged and the phase of their condensation products (precipitation and detrained cloud water) is determined after each scheme has operated. This method is energetically consistent, but does not capture the additional heat source for rising air parcels in convective updrafts provided by the latent heat of fusion (e.g., Williams and Renno 1993).

a. Stratiform clouds

The RK98 prognostic cloud water formulation was adopted in CAM2. For computational expediency, and since the latent heat of fusion was ignored prior to CAM3, that scheme used a total cloud condensate variable that combined the liquid and ice phases according to a temperature-dependent ice fraction. It is well known that the microphysical and radiative properties of ice and liquid are quite different. Ice particles sediment much more rapidly than cloud droplets because they grow to much larger size. These considerations have motivated our effort to separate cloud liquid and ice variables. Separating cloud liquid and ice allows us to track the energy associated with freezing and melting of cloud condensate, allows us to treat the differences in radiative properties and sedimentation more realistically, and provides hooks into these processes for improved representations in the future.

Advection of cloud condensate was ignored in CAM2 since the condensate tends to evolve on time scales that are fast compared to advection. However, ignoring advection of condensate resulted in total water not being conserved following the flow, even if no precipitate was formed. This is not a significant problem in most of the troposphere where much of the condensate formed in clouds is precipitated and the condensate mass is frequently a small component of the total water mass. In contrast, advection and sedimentation of cloud condensate should not be neglected in the tropical upper troposphere where the masses of the ice and vapor phases of water are similar and the lifetime of cloud ice is relatively long. Therefore, cloud liquid and ice mass mixing ratios are both advected in CAM3.

1) LIQUID AND ICE PARTITIONING

In the real world, the ice and liquid phases of condensate go through a complex interplay. The differences in saturation vapor pressure and the thermodynamics of phase change lead to a variety of processes (diffusion, collision, the Bergeron–Findeisen process, contact nucleation, splintering, evaporation, energy transitions, electrostatics, particle shape, etc.) that require an enormously complex set of equations to represent. While we intend to improve our representation of these processes in the future, we initially chose to remain close to the existing simple formulation.

Therefore, cloud liquid and ice are still assumed to coexist with a temperature dependent fraction

$$0 \le f_i = \frac{T - T_{\max}}{T_{\min} - T_{\max}} \le 1. \tag{2}$$

Each phase of water is transported separately, but after advection, convective detrainment, and sedimentation the liquid and ice are repartitioned according to (2) with the required heating accounted for. The RK98 parameterization, which governs the conversion from liquid and ice to rain and snow, can subsequently be used with very little modification. We did modify the forms described in RK98 and Zhang et al. (2003) by doubling the thresholds at which cloud ice begins converting to snow and including the heating associated with phase changes in the formulations for rain and snow production.

The bounds $T_{\min}$ and $T_{\max}$ are adjustable within a narrow range and the values in CAM3 are $-40°$ and $-10°$C, respectively. CAM2 had inconsistent temperature ranges for f_i, using $(-30°, -10°)$ for the radiative properties of clouds and $(-20°, 0°)$ for the microphysics.

Both the deep (ZM95) and shallow (H94) convection schemes form cloud condensate, which is either converted to precipitate or detrained into the stratiform cloud in CAM3. In CAM2, all of the detrained condensate from the H94 scheme and a fraction of that from the ZM95 scheme were assumed to evaporate into the environment rather than detraining into clouds. The phase of the detrained condensate is determined by (2) with the required latent heat of fusion added as a heating at the detrainment level (since the convection schemes do not account for freezing).

2) Particle sizes and sedimentation

The particle characterization for radiation and sedimentation was very simple in CCM3 and CAM2. Sedimentation of cloud particles was ignored. Ice particle optical radii were a function only of pressure. Those models assumed the cloud ice radius to be 10 μm below 800 mb and 30 μm above 400 mb with linear variation in pressure between those levels. Recent measurement and modeling studies (see Mitchell et al. 1996a,b) suggest that ice particle sizes are better characterized according to temperature. In CAM3, we have assumed that ice particle sizes are a function only of temperature, following Kristjánsson et al. (2000), as shown in Fig. 5.

The second moment of the cloud particle size distribution determines both the effective radius R_e for cloud optics (Mitchell 2002) and the mass-weighted radius for the sedimentation velocity. These radii are assumed to be the same in CAM3. For ice particles, both fall velocity and optical properties may be complicated functions of the crystal shapes. However, a single ice radius seems justified, given the simplicity of other aspects of the cloud microphysical and radiative treatments.

For cloud liquid drops, R_e can be calculated from the drop number density and liquid water mixing ratio. This quantity is calculated and used in the microphysics formulation. However, we still prescribe R_e for sedimentation and radiation in CAM3 to minimize changes in this aspect of the model. (The value calculated in the microphysics can be used with minor modifications to the code.) We have prescribed $R_e = 14$ μm over oceans, while R_e depends on T and snow depth over land. For $T > 0°$C, R_e is assumed to be 8 μm over land in the absence of snow. Here R_e increases linearly from 8 to 14 μm as snow equivalent water depth increases from 0 to 10 cm, or T decreases from 0° to $-20°$C. We also employ a 1000-km transition region between land and maritime regions. The R_e increases linearly from continental to oceanic values with distance from major land masses. This is intended to account for higher cloud drop numbers in coastal regions and is particularly important in the stratocumulus regions.

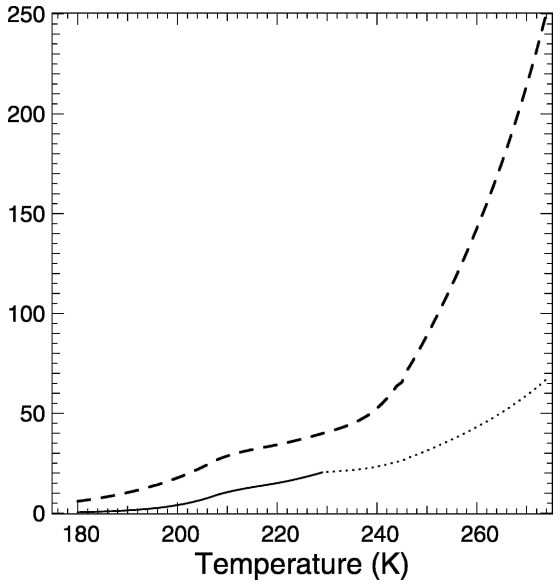

FIG. 5. Ice radius (μm, dashed) and fall velocity (cm s^{-1}) vs temperature. The ice velocity curve is solid where it is given by the Stokes terminal velocity and dotted where it is linear in radius.

Cloud liquid and ice particles sediment using independent settling velocities. Sedimenting particles evaporate if they fall into the cloud-free portion of a layer. As in the radiation, maximum overlap is assumed, so particles only evaporate if the cloud fraction is larger in the layer above. The settling velocity v is a function of the effective radius R_e. For $R_e < 40 \times 10^{-6}$ m, the Stokes terminal velocity equation for a falling sphere is used $v = (2/9)\rho_w g R_e^2/\eta$ where $\eta = 1.7 \times 10^{-5}$ kg m s^{-1} is the viscosity of air and the density of air has been neglected compared to ρ_w, the density of water. For $R_e > 40 \times 10^{-6}$ m, the Stokes formula is no longer valid and v increases linearly with R_e toward 1 m s^{-1} at $R_e = 400 \times 10^{-6}$ m, following Locatelli and Hobbs (1974, Fig. 6.6).

b. Evaporation and phase of precipitation

We calculate the fluxes of precipitation by assuming that precipitation is in a steady-state balance with its sources and sinks. The flux of precipitation at the top of the atmosphere is assumed to be zero. The flux of precipitation at the bottom of each layer F_b is then

$$F_b = F_t + \frac{\delta p}{g}(P - E) \tag{3}$$

where F_t is the flux at the top of the layer, P is the production term for precipitation, and E the evaporation term; F_b for the bottom layer is the surface precipitation and P is determined by the convection or stratiform microphysics. In the stratiform formulation P can be represented generally as the sum of six terms (RK98): autoconversion of cloud liquid to rain and cloud ice to snow, accretion of cloud liquid by rain and cloud ice by snow, and accretion of cloud liquid by snow and cloud ice by rain. The last two (mixed phase) terms involve freezing of the supercooled liquid and release of latent heat. The RK98 microphysics determines the first five production terms for stratiform clouds. The ZM95 and H94 convection schemes represent P entirely by the first term (autoconversion of liquid to rain). The evaporation of precipitation (rain plus snow) is computed for each source of precipitation following Sundqvist (1988):

$$E = k_e(1 - f)\left[1 - \min\left(1, \frac{q}{q^*}\right)\right](F_t)^{1/2}, \tag{4}$$

where k_e is an adjustable constant and f is the fractional cloud area, defined below. Note that precipitation is not permitted to evaporate in the layer in which it forms. The $(1 - f)$ factor represents a crude overlap assumption that uniformly distributed precipitation falling into the existing cloud in a layer does not evaporate. Here E is bounded to ensure that it does not supersaturate the layer and that it does not exceed the flux into the layer. For convective precipitation, $k_e = 1 \times 10^{-6}$ and, for stratiform precipitation, $k_e = 1 \times 10^{-5}$. Evaporation was included in the RK98 scheme and was added for ZM95 convection in CAM2 and for H94 convection in CAM3.

The precipitation phase in CAM2 was diagnosed from the near-surface temperatures. In CAM3, (3) also applies to snow with E scaled by the ratio (r_t) of the snow flux to the total precipitation flux at the layer top. Since the RK98 microphysics computes only one of the two mixed phase production terms, the net mixed phase production is taken as the greater of the available term (accretion of liquid by snow) and f_{snow} times the net rain production. Here f_{snow} decreases from 1 to 0 between $-5°$ and 0°C. Note that f_{snow} applies to the production term not the flux; once rain forms, it does not freeze. Convective snow production is given by $\max(r_t, f_{\text{snow}})\, P$, where $r_t P$ represents accretion of liquid by snow. All snow melts if it falls into a layer with $T > 0$°C.

c. Cloud fraction

Cloud fraction is determined diagnostically for convective and stratiform clouds. Although the general formulations of the cloud fractions are physically motivated, there are several adjustable constants that are determined empirically by constraining the top of atmosphere radiative budget.

Convective cloud fractions are determined separately for the deep and shallow convection schemes. Each depends on its respective convective mass flux $M_c^{d,s}$, as

$$0 \le f_c^{d,s} = c_1 \log(1 + c_2 M_c^{d,s}) \le f_{\max}^{d,s}. \tag{5}$$

The adjustable constants $c_1 \sim 0.1$ and $c_2 \sim 500$ are set separately for the two convection schemes. The upper bounds are $f_{\max}^d = 0.6$ and $f_{\max}^s = 0.3$. The total convective cloud fraction is $0 \le f_c = f_c^d + f_c^s \le 0.8$.

The fraction of a grid cell covered with convective cloud is assumed to be saturated, so the relative humidity outside of the convective cloud is $H' = (H - f_c)/(1 - f_c)$, where H is the cell average value. The stratiform cloud fraction f_s is determined as

$$0 \le f_s = \left(\frac{H' - H_{\min}}{1 - H_{\min}}\right)^2 < 1, \tag{6}$$

where the threshold $H_{\min}$ is an adjustable constant that depends on pressure. The main difference in CAM3, compared to CCM3 and CAM2, is that $H_{\min}$ does not have a stability dependence and $H_{\min} \le 0.91$ for all existing model configurations. In the previous models, the stability dependence resulted in $H_{\min} > 0.99$ over most of the tropical upper troposphere. Clouds then turned on or off abruptly due to minor variations in relative humidity.

As in CAM2 and CCM3, a marine stratus parameterization based on Klein and Hartmann (1993) gives a lower bound on f_s for cells that are at least one-half ocean covered. This parameterization is only active over limited regions off the west coasts of continents.

The total cloud fraction is given by $f = f_c + f_s < 1$. Neither the deep or shallow convection schemes determine cloud water content or other cloud properties. Therefore, f is used in the RK98 stratus cloud scheme instead of f_s, and all clouds are assigned the resulting water content and particle sizes. This approach is somewhat inconsistent and each scheme should be determining the properties of its own clouds.

5. Results

Results are shown here for a 6-yr simulation of CAM3 using the finite volume dynamical core at $2° \times 2.5°$ horizontal resolution. The revisions to the cloud

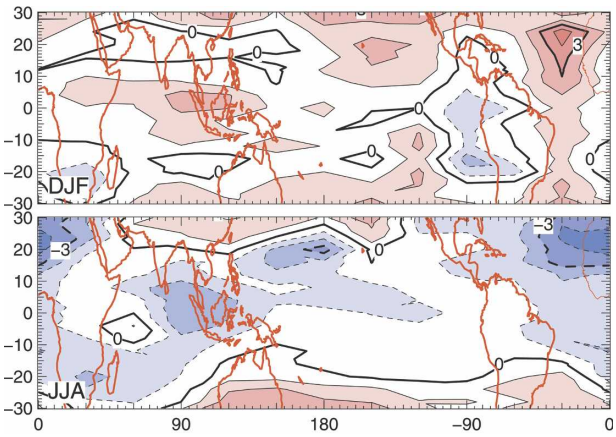

FIG. 6. CPT temperature bias for CAM3 compared to GPS/MET observations for (top) DJF and (bottom) JJA. The contour interval is 1 K.

treatment in CAM3 have warmed the tropical tropopause and virtually eliminated the CPT bias in CAM3 with respect to GPS/MET, as shown in Fig. 6. However, recalling that the GPS/MET observations are for a particularly cold year at the CPT (Randel et al. 2003), CAM3 probably still has a small cold bias. The simulation is nearly unchanged over South America and the Atlantic. Across the Indian and Pacific Oceans the CPT is 2–3 K warmer. The CPT remains slightly cold in JJA because CAM3 does not have sufficient vertical resolution to represent the seasonal cycle of the tropopause pressure. Tests have confirmed that the tropopause descends and warms in JJA if the vertical grid spacing is decreased to ~500 m.

Other aspects of the basic CAM3 simulation are discussed further in Collins et al. (2006b). The zonally averaged temperature bias in CAM3 is not greatly different from CAM2 outside the Tropics. In the Tropics, the whole profile of CAM3 is slightly warmer than CAM2, but the vertical structure is very similar. The largest bias remains the cold polar tropopause in summer, in common with previous versions of the model and, indeed, most GCMs.

Figure 7 shows the zonally averaged DJF cloud amount and ice fraction. Given that the dependence of ice fraction on temperature is specified by (2), it is not surprising that the transition from liquid cloud ($f_i = 0$) to ice cloud ($f_i = 1$) occurs between the −10°C and −40°C isotherms. The cloud fraction is similar to that in CAM2 (see Zhang et al. 2003). The largest cloud fractions are found in the lower troposphere at middle to high latitudes. The maximum in tropical cloud cover reaches 35% near 200 mb. These features are in reasonable agreement with observations and are discussed further in Hack et al. (2006). The most significant difference with respect to CAM2 is that there is more low and middle cloud in CAM3 due to the inclusion of (5) for convective cloud fractions.

The tropical cloud fraction decreases to <10% at 100 mb, suggesting that subvisible cirrus are underestimated in CAM3. Wang et al. (1996) found that subvisible cirrus clouds occurred >45% of the time just below

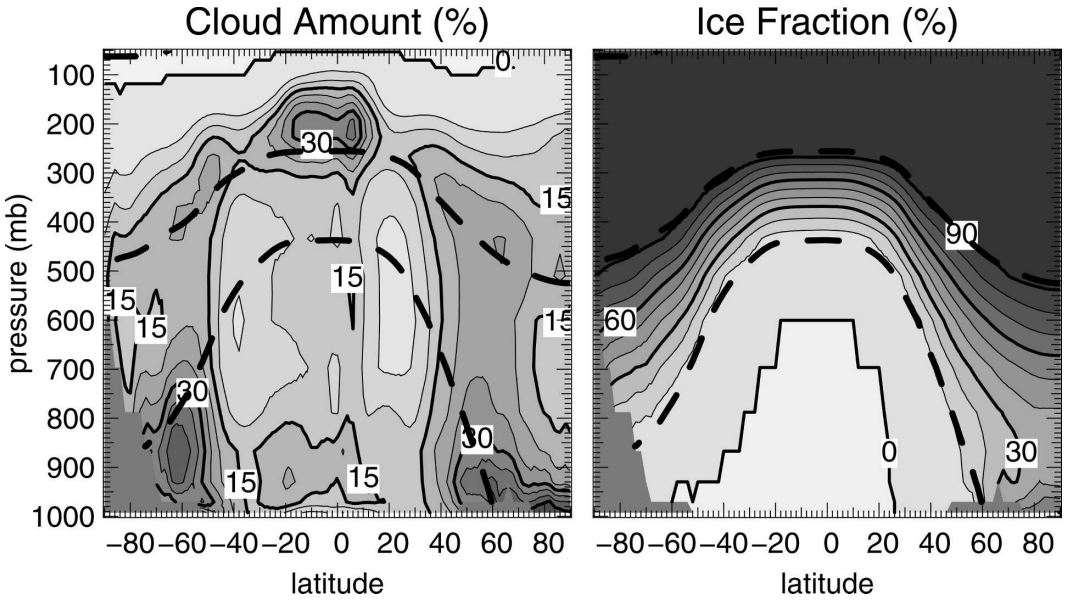

FIG. 7. DJF zonally averaged (left) cloud amounts (contour 5%) and (right) ice fraction (contour 10%). Heavy dashed lines show the −10° and −40°C isotherms.

the tropical tropopause in Stratospheric Aerosol and Gas Experiment II profiles, but the fractional area covered in each event cannot be determined. The cumulative probability distribution of tropopause level cirrus coverage in the vicinity of the Pacific warm pool is shown in Fig. 8. The CAM3 cloud distribution is quite smooth, only 27% of cells being completely clear and 1% being completely cloudy. However, this region has the highest average tropopause cloud fraction and yet only 50% of cells have $f > 0.05$ and 20% have $f > 0.25$ in CAM3. While the satellite observations of cloud frequency do not correspond to frequency distributions of cloud fraction, it seems almost certain that the cloud fraction is being underestimated in CAM3. This explains why CAM3 remains slightly cold compared to climatological estimates of CPT temperature (Seidel et al. 2001). While the cloud fraction is regarded as a tunable variable in CAM3, the formulation described in section 4c does not allow subvisible cirrus to be adjusted independently of other clouds. Decreasing $H_{\min}$ warms the tropopause further (and is done in upper atmosphere versions of CAM3 with interactive chemistry), but causes an imbalance in the top of atmosphere radiation due to increasing anvil clouds controlled by the same $H_{\min}$. Adding more adjustable constants to the cloud fraction parameterization does not seem advisable at the moment.

The discontinuous behavior of tropopause clouds in the earlier version of the model can also be seen in Fig. 8. CAM2 has only 1% cumulative probability of $0.01 < f < 0.99$, compared to 64% in CAM3. Most CAM2 grid cells are entirely clear (55%) or cloud covered (37%). The 7% of grid cells with $f = 0.01$ are due to an imposed value for cells where $0.99 < H < H_{\min}$.

The probability distribution for in-cloud (cell average/f) ice concentration is shown in Fig. 9. Typical tropopause ice concentrations in CAM3 are considerably higher than in CAM2, and are primarily responsible for the warming of the CPT with respect to CAM2. Ice concentrations are larger in CAM3 in large part because the cloud fraction varies more smoothly. In the RK98 scheme as modified by Zhang et al. (2003), the evaporation rate increases as the ice concentration increases due to decreasing f. If f decreases slowly, the excess cloud ice will evaporate back into the environment. However, if f decreases rapidly, the spike of the in-cloud ice concentration will exceed the autoconversion threshold and form precipitation before evaporation can deplete the cloud ice. The autoconversion threshold in CAM2 (5 ppmm) can be clearly seen as a spike in the frequency distribution in Fig. 9. The CAM3 threshold (9.5 ppmm) is less obvious, but can also be seen. Although greatly reduced, CAM3 still has a problem with decreasing f causing large in-cloud ice and formation of precipitate. This is believed to be unrealistic and alternative formulations for relating variations in f to cloud concentrate variations will be explored.

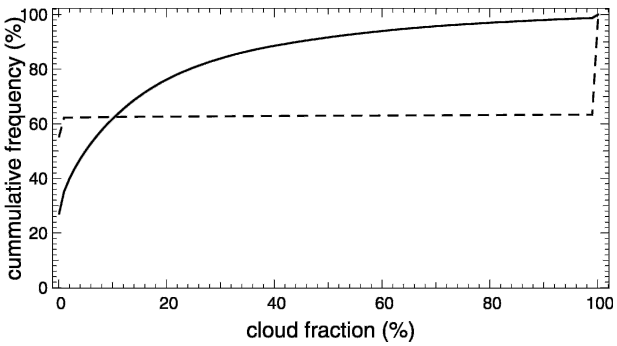

FIG. 8. Cumulative probability distribution for cloud fraction at 85 mb in the region 20°S–20°N, 120°–150°E. The solid (dashed) line shows CAM3 (CAM2), sampled hourly for January.

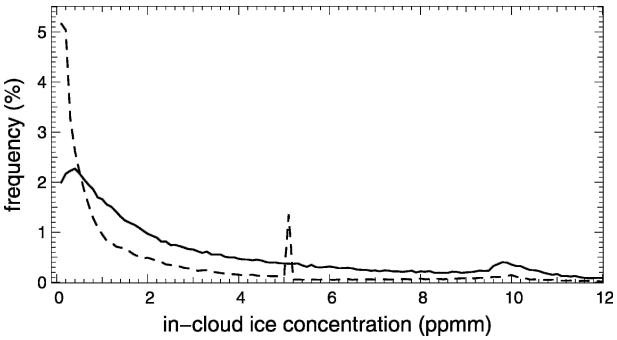

FIG. 9. As in Fig. 8 except that the probability density function for in-cloud ice concentration (ppmm) is shown.

Figure 10 shows the cloud ice and water mixing ratios. Cloud liquid is found mostly below the −10°C isotherm. Compared to RK98, there is much more cloud liquid, particularly in higher latitudes of the Southern Hemisphere. Cloud ice is found mostly in the middle of the (−10°, −40°C) temperature range, where much of the condensate is in ice form and there is still enough total water to make relatively thick ice clouds. One of the major sensitivities of the CAM3 cloud formulation is to the specification of the temperature bounds in (2). Shifting the warm bound from −10° to 0°C will decrease the liquid water loading, with a much smaller increase in ice water loading. Cloud liquid remains in the atmosphere longer than ice because it falls more slowly and converts to precipitation less effectively.

Figure 11 shows the ice and liquid condensate sources from convective detrainment and from the net of condensation–evaporation in stratiform cloud. Ice detrainment occurs mostly between 200–400 mb in the

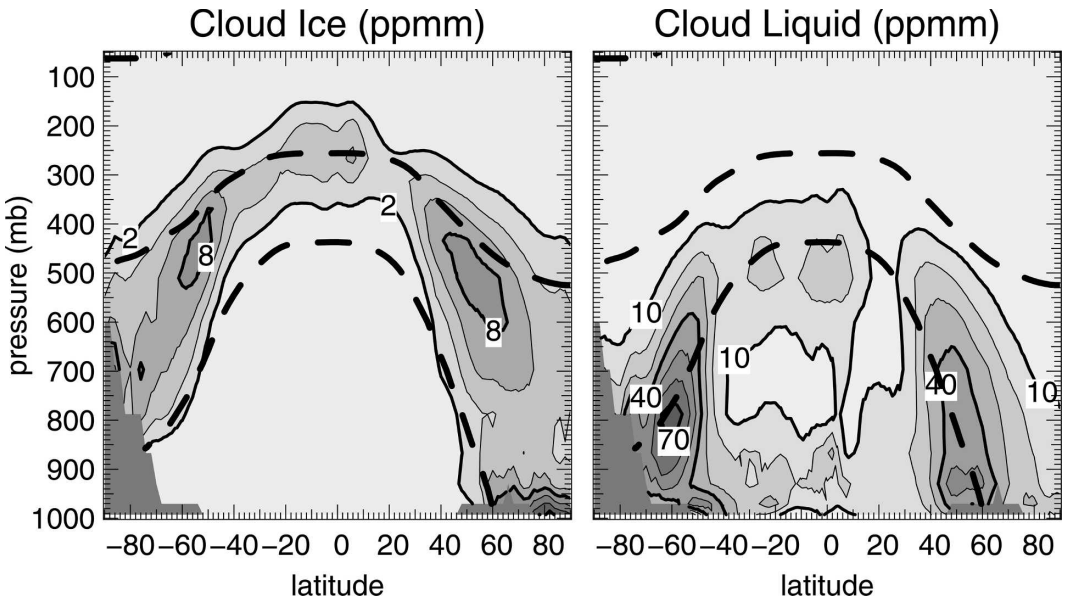

FIG. 10. As in Fig. 7, except that (left) cloud ice (contour 2 ppmm) and (right) cloud liquid (contour 10 ppmm) mixing ratios are shown.

Tropics. At lower levels, liquid condensate is detrained from deep convection in the Tropics. At all latitudes, there is a substantial liquid condensate source from detrainment by shallow convection below 700 mb. In fact, detrainment from shallow convection is the largest source of cloud liquid in CAM3. Although this term was always computed by the H94 convection, the detrained liquid was assumed to evaporate in previous model versions. Where the detrainment terms are large, they tend to be partly compensated for by evaporation of condensate in stratiform clouds. Condensation in stratiform clouds occurs mostly in regions where the detrainment source is small.

Figure 12 shows the heating from the original H94 and ZM95 convection parameterizations and the heating from the terms that have been added in CAM3: evaporation of precipitation and snow production and melt; and the latent heat of fusion associated with the detrainment of cloud ice. H94 convection is primarily shallow and is largest in the extratropics. However, there is a significant contribution from H94 convection in the Tropics between ~400 and ~200 mb, where it is comparable to the ZM95 convective heating. ZM95 convection is mostly confined to the Tropics.

Heating by the additional freezing and evaporation processes are relatively minor compared to the original parameterized heating. For example, the heat source from detrainment of ice reaches 1 mW kg^{-1} in the Tropics near 300 mb where the convective heating is ~10 mW kg^{-1}. The cooling from snowmelt and evaporation reaches ~6 mW kg^{-1} at 600 mb where the convective heating is ~27 mW kg^{-1}. However, snowmelt and evaporation systematically cool (destabilize) the middle troposphere, while snow production and ice detrainment systematically heat the upper troposphere. The heating associated with freezing should cause the convection to penetrate deeper, but it is likely that the opposite is occurring. The heating is actually taking place in the environment outside the convection, making the upper troposphere slightly more stable.

Figure 13 shows the net heating due to all convective processes (the sum of the four panels in Fig. 12) and due to stratiform processes. Convective heating is generally much stronger than stratiform heating. In fact, the stratiform processes actually cool over most of the lower and middle troposphere owing to evaporation of detrained water from the convection. The major exception is in the middle troposphere at middle latitudes where ice formation in stratus clouds provides significant heating.

Figure 14 shows the total precipitation and snow, together with the contributions from convection and stratus clouds. Middle and high latitude precipitation is dominated by stratiform processes, with snow coming almost entirely from stratus clouds. The shallow convection plays a crucial role in detraining water into the stratus clouds, but does not contribute directly to precipitation.

Tropical precipitation is dominated by convection, mostly due to ZM95 convection. H94 convection is negligible in the precipitation budget, with a maximum zonally averaged DJF precipitation rate of 0.13 mm day^{-1}.

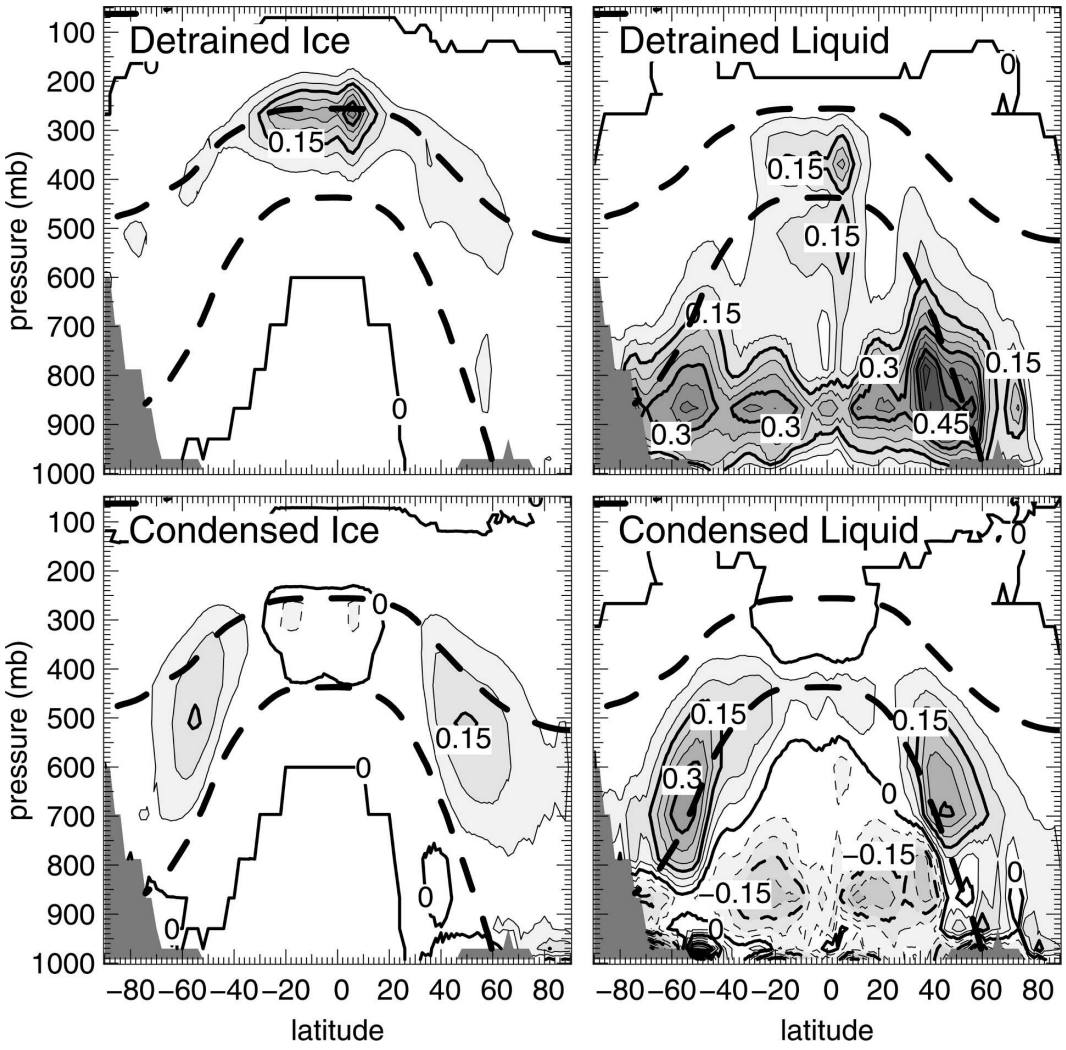

FIG. 11. DJF zonally averaged (left) cloud ice and (right) cloud liquid source terms from (top) convective detrainment and (bottom) condensation minus evaporation. The contour interval is 0.05 g kg^{-1} day^{-1}. Heavy dashed lines show the −10° and −40°C isotherms.

What little stratiform precipitation is produced in the Tropics mostly evaporates before it hits the ground. Only ~10% of tropical precipitation comes from stratus clouds, in contrast with observations which find that ~50% of the tropical precipitation comes from stratus clouds, including anvils (e.g., Houze 1997; Schumacher and Houze 2003). Anvils are considered stratiform cloud in CAM3 and are fed by detrained water from convection. This suggests that the detrainment of condensate is significantly underestimated in the ZM95 convection scheme. Most of the condensed water is (auto) converted to precipitation in the cumulus towers below 600 mb and only a small fraction is detrained into the anvils. In fact, no detrainment is permitted in the ZM95 scheme below 500 mb. Experiments in which the autoconversion rate was reduced lead to excessive detrainment near 500 mb.

6. Conclusions

Several improvements have been made to the treatment of cloud processes in CAM3, particularly with respect to the cloud condensate. Much of this work was motivated by the analysis of a ~3 K cooling of the tropical tropopause that occurred between CCM3 and CAM2. This bias resulted from the combination of three parameterization changes between CCM3 and CAM2, although each change is believed to make the parameterization more realistic than the earlier version. Indeed, the parameterization changes did result in

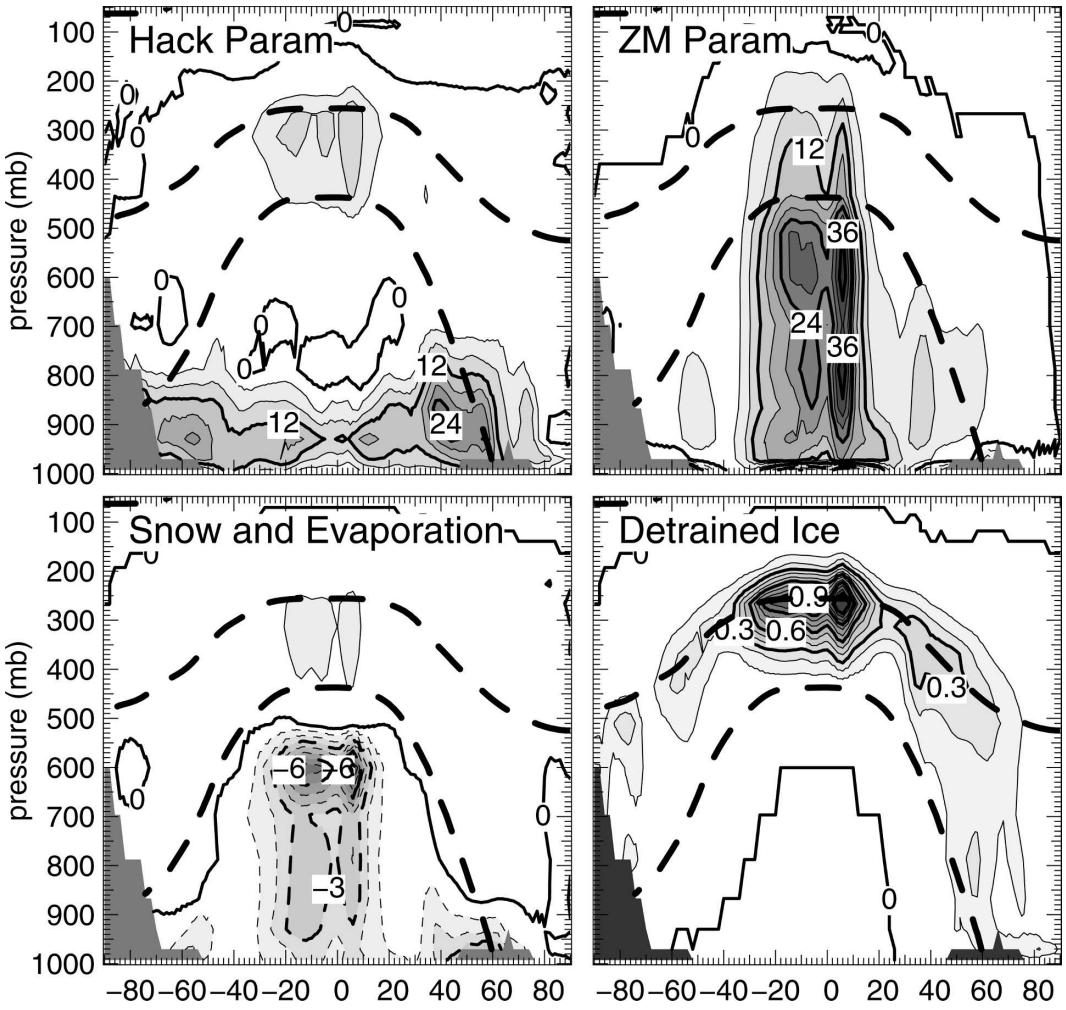

FIG. 12. DJF zonally averaged heating due to (top left) H94 and (top right) ZM95 convection, contour 4 mW kg^{-1}; (bottom left) net convective snow production, melt, and evaporation of precipitation, contour 1 mW kg^{-1}; and (bottom right) ice detrainment, contour 0.2 mW kg^{-1}.

improvements in other aspect of the CAM2 simulation, such as, increased tropical lower tropospheric humidity. Radiative equilibrium calculations showed that increasing the cloud water content to realistic levels in the tropical upper troposphere could remove the tropopause cold bias. This motivated a reexamination of the clouds and precipitation processes in CAM in order to improve the representation of cloud condensate, especially cloud ice.

The physical basis of the treatment of clouds and precipitation processes has been considerably improved in CAM3, compared to both CAM2 and CCM3, and several inconsistencies in the formulation of the earlier models have been removed. Cloud ice and liquid condensate are treated as separate variables in CAM3, and both variables are advected by the large scale circulation and undergo gravitational settling. Particle sizes are determined consistently in the microphysical and radiation parameterizations. Snowfall is computed explicitly, and the latent of fusion has been included for all freezing and melting processes. Both deep (ZM95) and shallow (H94) convection parameterizations now detrain cloud condensate directly into the stratus clouds.

The tropical tropopause temperature has been greatly improved in CAM3, almost entirely due to a better representation of cloud ice near the tropopause. This result is likely to be quite general: the radiative effects of subvisible cirrus are powerful enough that obtaining a realistic tropopause will require an accurate simulation of the subvisible cirrus area and ice concentration. CCM3 was able to obtain reasonable tropopause temperatures, partly because the ice concentrations were specified and partly due to other compen-

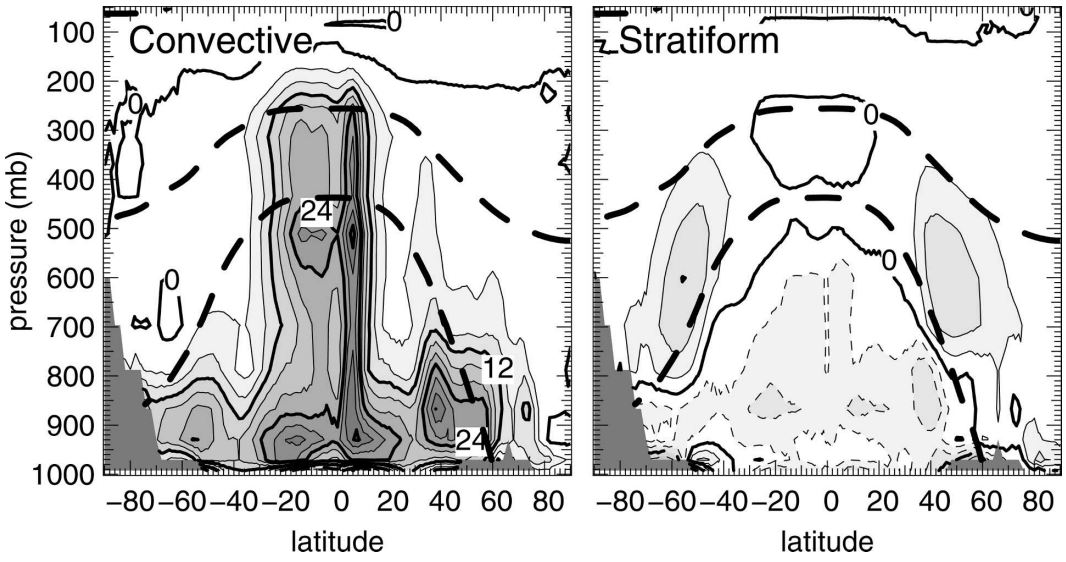

FIG. 13. DJF zonally averaged net heating due to all (left) convective process and (right) stratiform processes. The contour interval is 4 mW kg^{-1}.

sating errors. CAM3 obtains this result through a radiative budget that is believed to be more realistic: increased ice concentrations near the tropopause provide heating that compensates for a decrease in the upwelling longwave flux due to a better representation of clouds and humidity lower down.

Explicitly treating all phase conversions and including the latent heat of fusion has eliminated the globally averaged energy loss of ~0.2 W m^{-2} due to inconsistencies between the atmospheric and surface models, discussed by Boville and Gent (1998) and Boville and Bretherton (2003). The effect of the latent heat of fusion on the CAM3 simulation is relatively modest because the latent heat of fusion is small compared to the latent heat of vaporization. Therefore, adding the heat due to the freezing of cloud condensate modifies the convective heating by <20%. However, this term might make a larger difference if it was included within the formulation of the convective parameterizations.

The principal remaining problems with the treatment of clouds are believed to be 1) the diagnostic determination of cloud fraction, 2) the specification of the cloud ice fraction purely as a function of temperature, and 3) the number density and size of cloud particles being determined independently of the cloud water content. Initial tests of a consistent treatment for the calculation of the cloud particle size have already been conducted and this work is expected to be included in the next version of CAM. Improvements to the stratus clouds microphysics are also being developed.

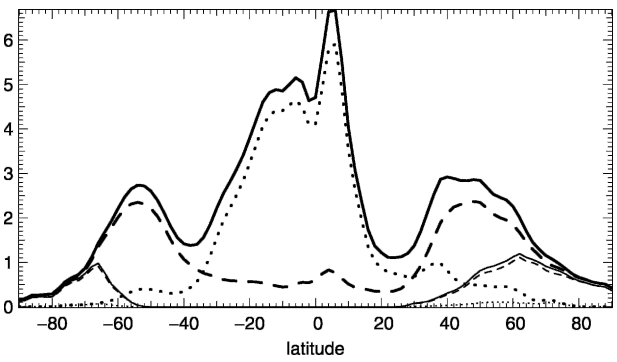

FIG. 14. DJF zonally averaged total precipitation (thick, mm day^{-1}) and snow (thin) from all sources (solid), convection (dotted) and stratus (dashed).

Acknowledgments. Numerous conversations between PJR and Mark Lawrence and Jan Egel Kristjánsson, and between BAB and Rolando Garcia and Andrew Gettelman greatly aided in this work. Part of this work was supported under NASA GMAP Grants W-19, 764 and NNH04AB421. Two anonymous reviews contributed to substantial improvements to the original manuscript.

REFERENCES

Boville, B. A., and P. R. Gent, 1998: The NCAR climate system model, version one. *J. Climate,* **11,** 1115–1130.

——, and C. S. Bretherton, 2003: Heating and kinetic energy dissipation in the NCAR Community Atmosphere Model. *J. Climate,* **16,** 3877–3887.

——, J. T. Kiehl, P. J. Rasch, and F. O. Bryan, 2001: Improvements to the NCAR CSM-1 for transient climate simulation. *J. Climate,* **14,** 164–179.

Collins, W. D., 2001: Parameterization of generalized cloud overlap for radiative calculations in general circulation models. *J. Atmos. Sci.,* **58,** 3224–3242.

——, J. K. Hackney, and D. P. Edwards, 2002: A new parameterization for infrared emission and absorption by water vapor in the National Center for Atmospheric Research Community Atmosphere Model. *J. Geophys. Res.,* **107,** 4664, doi:10.1029/2001JD001365.

——, and Coauthors, 2006a: The Community Climate System Model version 3 (CCSM3). *J. Climate,* **19,** 2122–2143.

——, and Coauthors, 2006b: The formulation and atmospheric simulation of the Community Atmosphere Model version 3 (CAM3). *J. Climate,* **19,** 2144–2161.

——, J. M. Lee-Taylor, D. P. Edwards, and G. L. Francis, 2006c: Effects of increased near-infrared absorption by water vapor on the climate system. *J. Geophys. Res.,* in press.

Dessler, A. E., 1998: A reexamination of the "stratospheric fountain" hypothesis. *Geophys. Res. Lett.,* **25,** 4165–4168.

Hack, J. J., 1994: Parameterization of moist convection in the NCAR Community Climate Model, CCM2. *J. Geophys. Res.,* **99** (D3), 5551–5568.

——, J. Caron, S. Yeager, K. Oleson, M. Holland, J. Truesdale, and P. J. Rasch, 2006: Simulation of the global hydrological cycle in the CCSM Community Atmosphere Model version 3 (CAM3): Mean features. *J. Climate,* **19,** 2199–2221.

Hartmann, D. L., J. R. Holton, and Q. Fu, 2001: The heat balance of the tropical tropopause, cirrus, and stratospheric dehydration. *Geophys. Res. Lett.,* **28,** 1969–1972.

Holloway, J. L., and S. Manabe, 1971: Simulation of climate by a global general circulation model. 1. Hydrologic cycle and heat balance. *Mon. Wea. Rev.,* **99,** 335–370.

Holton, J. R., and A. Gettelman, 2001: Horizontal transport and the dehydration of the stratosphere. *Geophys. Res. Lett.,* **28,** 2799–2802.

——, P. H. Haynes, M. E. McIntyre, A. R. Douglass, R. B. Rood, and L. Pfister, 1995: Stratosphere–troposphere exchange. *Rev. Geophys.,* **33,** 403–439.

Holtslag, A. A. M., and B. A. Boville, 1993: Local versus nonlocal boundary-layer diffusion in a global climate model. *J. Climate,* **6,** 1825–1842.

Houze, R. A., 1997: Stratiform precipitation in regions of convection: A meteorological paradox? *Bull. Amer. Meteor. Soc.,* **78,** 2179–2196.

Kiehl, J. T., J. J. Hack, G. B. Bonan, B. A. Boville, D. L. Williamson, and P. J. Rasch, 1998: The National Center for Atmospheric Research Community Climate Model: CCM3. *J. Climate,* **11,** 1131–1149.

Klein, S. A., and D. L. Hartmann, 1993: The seasonal cycle of low stratiform clouds. *J. Climate,* **6,** 1587–1606.

Kristjánsson, J. E., J. M. Edwards, and D. L. Mitchell, 2000: Impact of a new scheme for optical properties of ice crystals on climates of two gems. *J. Geophys. Res.,* **105,** 10 063–10 079.

Lin, S.-J., 2004: A "vertically Lagrangian" finite-volume dynamical core for global atmospheric models. *Mon. Wea. Rev.,* **132,** 2293–2307.

Locatelli, J. D., and P. V. Hobbs, 1974: Fall speeds and masses of solid precipitation particles. *J. Geophys. Res.,* **79,** 2185–2197.

McFarlane, N. A., 1987: The effect of orographically excited gravity wave drag on the general circulation of the lower stratosphere and troposphere. *J. Atmos. Sci.,* **44,** 1775–1800.

McFarquhar, G. M., A. J. Heymsfield, J. Spinhirne, and B. Hart, 2000: Thin and subvisual tropopause tropical cirrus: Observations and radiative impacts. *J. Atmos. Sci.,* **57,** 1841–1853.

Mitchell, D. L., 2002: Effective diameter in radiation transfer: General definition, applications, and limitations. *J. Atmos. Sci.,* **59,** 2330–2346.

——, S. K. Chai, Y. Liu, A. J. Heymsfield, and Y. Dong, 1996a: Modeling cirrus clouds. Part I: Treatment of bimodal size spectra and case study analysis. *J. Atmos. Sci.,* **53,** 2952–2966.

——, Y. Liu, and A. Macke, 1996b: Modeling cirrus clouds. Part II: Treatment of radiative properties. *J. Atmos. Sci.,* **53,** 2967–2988.

Randel, W. J., F. Wu, and W. R. Rios, 2003: Thermal variability of the tropical tropopause region derived from GPS/MET observations. *J. Geophys. Res.,* **108,** 4024, doi:10.1029/2002JD002595.

Rasch, P. J., and J. E. Kristjánsson, 1998: A comparison of the CCM3 model climate using diagnosed and predicted condensate parameterizations. *J. Climate,* **11,** 1587–1614.

——, and Coauthors, 2006: Characterization of tropical transient activity in the CAM3 atmospheric hydrologic cycle. *J. Climate,* **19,** 2222–2242.

Rosenfield, J. E., D. B. Considine, M. R. Schoeberl, and E. V. Browell, 1998: The impact of subvisible cirrus clouds near the tropical tropopause on stratospheric water vapor. *Geophys. Res. Lett.,* **25,** 1883–1886.

Sassi, F., B. A. Boville, R. R. Garcia, and D. Kinnison, 2005: The effects of interactive ozone chemistry in simulations of the middle atmosphere. *Geophys. Res. Lett.,* **32,** L07811, doi:10.1029/2004GL022131.

Schumacher, C., and R. A. Houze, 2003: Stratiform rain in the Tropics as seen by the TRMM precipitation radar. *J. Climate,* **16,** 1739–1756.

Seidel, D. J., R. Ross, J. Angell, and G. Reid, 2001: Climatological characteristics of the tropical tropopause as revealed by radiosondes. *J. Geophys. Res.,* **106,** 7857–7878.

Sherwood, S. C., 2000: A "stratospheric drain" over the maritime continent. *Geophys. Res. Lett.,* **27,** 677–680.

Sundqvist, H., 1988: Parameterization of condensation and associated clouds in models for weather prediction and general circulation simulation. *Physically-based Modeling and Simulation of Climate and Climate Change,* Vol. 1, M. E. Schlesinger, Ed., Kluwer Academic, 433–461.

Wang, P.-H., P. Minnis, M. P. McCormick, G. S. Kent, and K. M. Skeens, 1996: A 6-year climatology of cloud occurrence frequency from stratospheric aerosol and gas experiment. ii: Observations (1985–1990). *J. Geophys. Res.,* **101,** 29 407–29 430.

Williams, E., and N. Renno, 1993: An analysis of the conditional instability of the tropical atmosphere. *Mon. Wea. Rev.,* **121,** 21–36.

Williamson, D. L., 2002: Time-split versus process-split coupling of parameterizations and dynamical core. *Mon. Wea. Rev.,* **130,** 2024–2041.

——, and J. G. Olson, 1994: Climate simulation with semi-Lagrangian version of the NCAR Community Climate Model. *Mon. Wea. Rev.,* **122,** 1594–1610.

Zhang, G. J., and N. A. McFarlane, 1995: Sensitivity of climate simulations to the parameterization of cumulus convection in the Canadian Climate Centre general circulation model. *Atmos.–Ocean,* **33,** 407–446.

Zhang, M., W. Lin, C. S. Bretherton, J. J. Hack, and P. J. Rasch, 2003: A modified formulation of fractional stratiform condensation rate in the NCAR Community Atmospheric Model (CAM2). *J. Geophys. Res.,* **108,** 4035, doi:10.1029/2002JD002523.